Bulletin of Engineering Geology and the Environment
https://doi.org/10.1007/s10064-021-02449-2

ORIGINAL PAPER

Numerical prediction of undrained cyclic triaxial experiments on saturated Kasai river sand using two constitutive models of liquefaction

Raj Banerjee[1] · Rana Chattaraj[2] · Y. M. Parulekar[3] · Aniruddha Sengupta[4]

Received: 21 January 2021 / Accepted: 10 September 2021

Abstract

The paper presents a numerical simulation of stress-controlled undrained cyclic tri-axial tests conducted on local sand at various relative densities and CSR values. Two constitutive models for liquefaction, namely, Finn-Byrne model and PM4 sand model are used for the simulation. The results from both the material models are compared with the cyclic test results in terms of the stress strain loops, excess pore pressure ratio, and effective stress path. The chosen models have shown good predicting capabilities for predicting cyclic responses of a sand in terms of stress path and pore water pressure generation but lacks in predicting the stress strain behavior. Also, in terms of simulating the behavior of sand in pre- and post-liquefaction regime, it is found that PM4 sand model is more efficient than Finn model for all the relative densities. Hence, it is recommended that Finn model may be only utilized when a sand fails due to flow liquefaction, whereas PM4 sand model can predict both, flow liquefaction and cyclic mobility, accurately. Finally, the liquefaction resistance curves for different relative densities are obtained using experimental values and PM4 sand model. These curves are thus proposed for any sand with index properties similar to the particular sand considered for the study.

Keywords Cyclic triaxial test · Liquefaction · Finn-Byrne model · PM4 sand model

Introduction

Liquefaction is defined as a loss of strength of a loose saturated sand under cyclic loading (Jefferies and Been 2015). The loss of strength of a sand is known to cause considerable damage to existing man-made and earthen structures, which in turn is responsible to cause serious loss of human lives (Shou and Wang 2003; Stark and Contreras 1998).Hence, understanding of the phenomena known as "liquefaction" is of prime importance, and it is essential to numerically study this phenomenon by means of developing different constitutive models. Several roads, bridges, and buildings are being built (or planned to be built) on top of the saturated foundation local sand in the region of Kharagpur, India; hence, it becomes a necessity to understand the seismic behavior of the soil over which the structures are resting both experimentally and numerically. A set of the monotonic and cyclic triaxial tests of the present sand has been conducted experimentally for various relative densities, and the results are reported in a companion paper by Chattaraj and Sengupta (2016). However, numerical prediction of the experiments was not carried out by them, and it is essential to simulate the experiments in order to gain knowledge about selection of proper constitutive soil models to accurately predict liquefaction. Moreover, the description of the modes of failure of the sample during cyclic loading (flow liquefaction, cyclic mobility or limited flow liquefaction) was also not

✉ Raj Banerjee
rbanerjee@barc.gov.in

Rana Chattaraj
rana.chattarajfce@kiit.ac.in

Y. M. Parulekar
yogitap@barc.gov.in

Aniruddha Sengupta
sengupta@civil.iitkgp.ac.in

1 Bhabha Atomic Research Centre, 400085 Mumbai, India

2 Department of Civil Engineering, Kalinga Institute of Industrial Technology, 751024 Bhubneswar, India

3 Bhabha Atomic Research Centre, Homi Bhabha National Institute, 400085 Mumbai, India

4 Department of Civil Engineering, Indian Institute of Technology, 721302 Kharagpur, India

Published online: 27 September 2021

mentioned by them. Hence, in the present study, an extension of the work reported by Chattaraj and Sengupta (2016) is carried out which will help to identify a proper constitutive model of the foundation sand and predict the essential features of the accurate behavior of soil during cyclic loading.

In the initial developments, Ghaboussi and Dikmen (1978) have used a combination of a simple plasticity model for shear deformations, a rule to make changes in the effective stresses in a soil and a modified form of Masing rule to account for the degradation of soil stiffness during cyclic loading and pore water pressure generation. Similarly, Zienkiewicz et al. (1978) have proposed a non-associated Mohr–Coulomb elastoplastic model for shear behavior coupled with an additional expression determining the cumulative increase of the volumetric strain during a cyclic loading. The models proposed by Aubry et al. (1982) use a combined multi-mechanism model based on the framework proposed by Mroz (1967) for modeling cyclic response. Prevost (1985) has proposed a simple model based on the framework of multi-surface plasticity to predict the liquefaction of a sand. In addition to these models, a loosely coupled simple elastoplastic liquefaction model was proposed by Finn and its collaborators to predict the liquefaction behavior of a cohesionless soil. An improvement of the Finn model has been proposed by Beaty and Byrne (1998) in which elastoplastic hardening and a shear-induced dilation law have been introduced to better predict the dynamic responses of a soil during liquefaction. A significant improvement of the Prevost's multi-surface plasticity model has been performed by Elgamal and its collaborators (Parra 1996; Elgamal et al. 2002; Yang et al. 2003) for the analysis of soil liquefaction. A hypoplastic constitutive model implemented in three-dimension for ganular materials was proposed by Wu et al. (1996), and the model efficiently captured the significant features of saturated soil in monotonic and cyclic loading. A few years later, an efficient critical state model was proposed by Manzari and Dafalias (1997) which is capable of modeling the monotonic and the cyclic responses of sands. This model by Manzari and Dafalias (1997) is modified to include the fabric effects on liquefaction resistance of sand (Dafalias and Manzari 2004). This model is further refined to better predict the post liquefaction responses of soil in cyclic loading (Ziotopoulou and Boulanger 2013).

All the above-stated models have certain capabilities and limitations in the prediction of the soil liquefaction behavior which depends on various assumptions and therefore lead to realistic results only if these assumptions have some relationship to the physical behavior of the soil. Furthermore, in all the model developments, priority has been given to a single-constitutive model in terms of its capabilities and limitations for predicting the behavior of sand during and after liquefaction. But limited number of studies has been conducted to compare the results of these material models. One such notable work has been by Ramirez et al. (2018) in which the results from cyclic tests and a centrifuge model test performed on Ottawa sand are compared with those obtained from different liquefaction models namely PMDY02 and SANISAND model sand; these numerical models' capabilities and limitations have been highlighted. Chen et al. (2020) have calibrated the cyclic simple shear test results on Ottawa F65 sand using two liquefaction models — MD04 and PM4 sand models in plane strain and axisymmetric conditions. The usefulness and limitations of the two models have been highlighted in their work. Carey and Kutter (2017) have also compared the capabilities and limitations of various constitutive models (namely PM4 sand, UBC sand, PMDY02 and DM04 models) on a hypothetical sand. Zarrabi and Yniesta (2019) have compared the results of various bounding surface plasticity models on sandy and clayey soils with strain hardening and softening characteristics and have briefly discussed the merits and limitations of each model used in their study. Some more comparisons between the liquefaction models for sand and clay can be found in other works (Eslami et al. 2019; Yang et al. 2018). Other than element tests, the predictive capabilities and limitations of the developed constitutive models have been evaluated by centrifuge tests conducted as a part of verification of liquefaction analysis by centrifuge studies (VELACS) (Arulanandan and Scott 1993, 1994) and liquefaction experiments and analysis projects (LEAPs) (Kutter et al. 2015). However, all these studies were not carried out on local Indian type sand with varying relative densities.

In this study, an attempt has been made to compare the results of stress-controlled undrained cyclic tests conducted on a local sand (Kasai river sand) with those obtained from two constitutive models, namely, Finn-Byrne pore pressure formulation (Finn et al. 1977) with Mohr–Coulomb model implemented in FLAC 2D (Itasca 2005) and PM4 sand model (Ziotopoulou and Boulanger 2013) implemented in MIDAS GTS NX (2019). It is found that the significant parameters observed in pre- and post-liquefaction response during experiments are reflected accurately in PM4 sand model; hence, this model is recommended than Finn-Byrne model for the seismic behavior of liquefaction-induced failures and SSI analyses.

Experimental program and properties of foundation soil

The undrained stress-controlled cyclic tri-axial tests were performed on local sand specimens obtained from lower Ganga plane (70 mm in diameter and 140 mm in height), in accordance with ASTM D5311 (2011) to obtain the liquefaction potential of the sand (Chattaraj and Sengupta 2016).

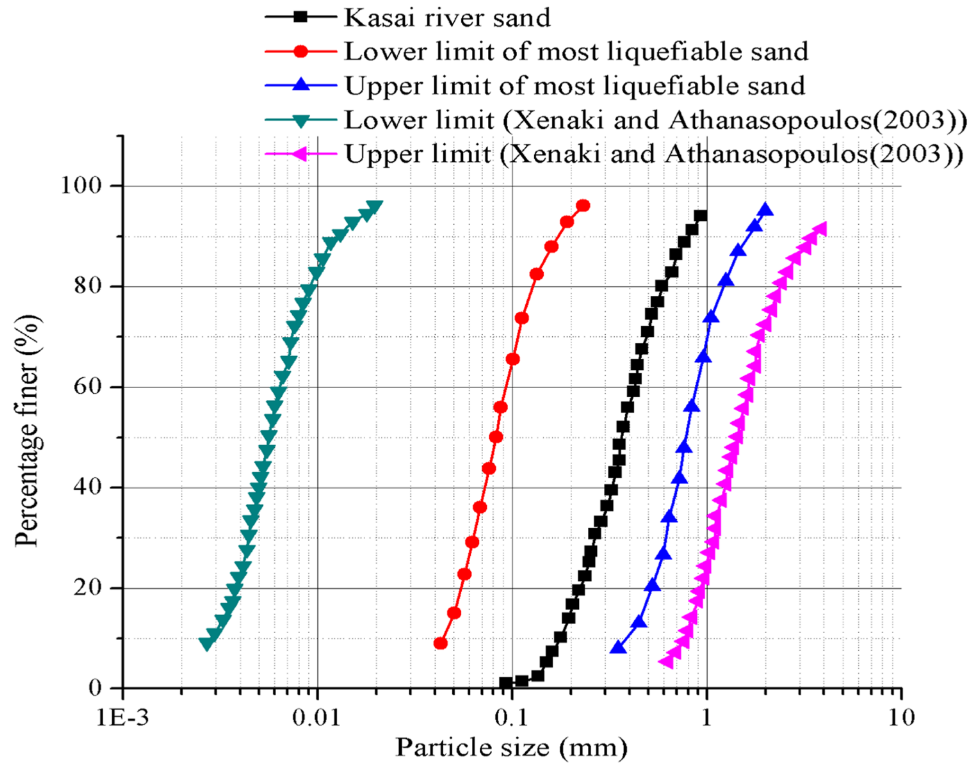

Fig. 1 GSD of the sand along with the liquefaction susceptibility ranges

The local sand known as Kasai (a short name of Kangsabati) River sand originates in the hills of Chattisgarh near Ranchi and flows through the edge of Chhotonagpur plateau and enters in the district Paschim Medinipur, conjoined with Keleghai and falls into the Haldi river. The Kasai river sand composes of 0.3% fines content, 1.7% coarse sand, 44% medium sand, and 54% of fine sand and is characterized as poorly graded sand as per Unified Soil Classification System. The angularity and the sphericity of the sand grains are found to be 0.82 and 0.78 (Chattaraj and Sengupta 2016). In order to preliminarily assess the liquefaction susceptibility of the Kasai river sand, the grain size distribution (GSD) as well as the range of gradation for a liquefiable sand, as given by Xenaki and Athanasopoulos (2003), is shown in Fig. 1.

It may be observed that the saturated sand used in the present work is very much susceptible to liquefaction.

Table 1 Material properties of the sand

Parameters for the sand	Value
Specific gravity	2.64
D_{10}, D_{30}, D_{60}	0.20, 0.32, 0.47
e_{max}	0.83
e_{min}	0.56
Coefficient of uniformity (C_u)	2.36
Coefficient of curvature (C_c)	1.08
Mass (saturated) density (kg/m^3)	1928

Table 1 shows all the material and the index properties for the sand. The drained peak friction angle (φ_{dp}) has been obtained from the isotropic consolidated drained (ICD) tri-axial tests on the river sand conducted at 100 kPa confining pressure for RD of 25%, 40%, 60%, and 80%, and the results are plotted in Fig. 2. Also, the undrained effective friction angle (ϕ_{up}) has been obtained from the isotropic consolidated undrained (ICU) tri-axial tests on the river

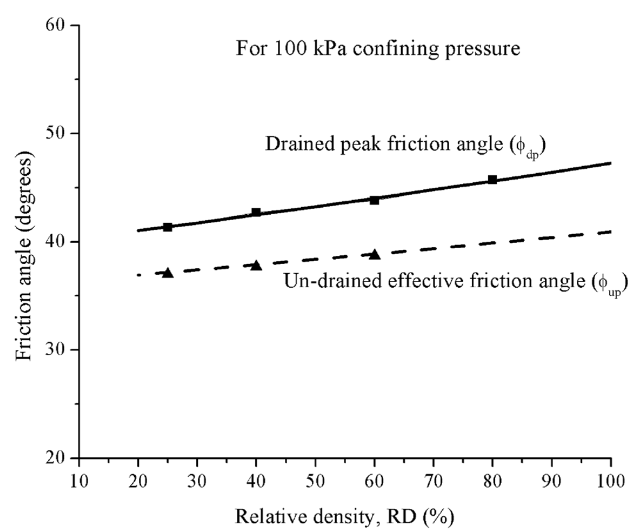

Fig. 2 Variation of drained and undrained friction angle with relative density (RD) for Kasai river sand

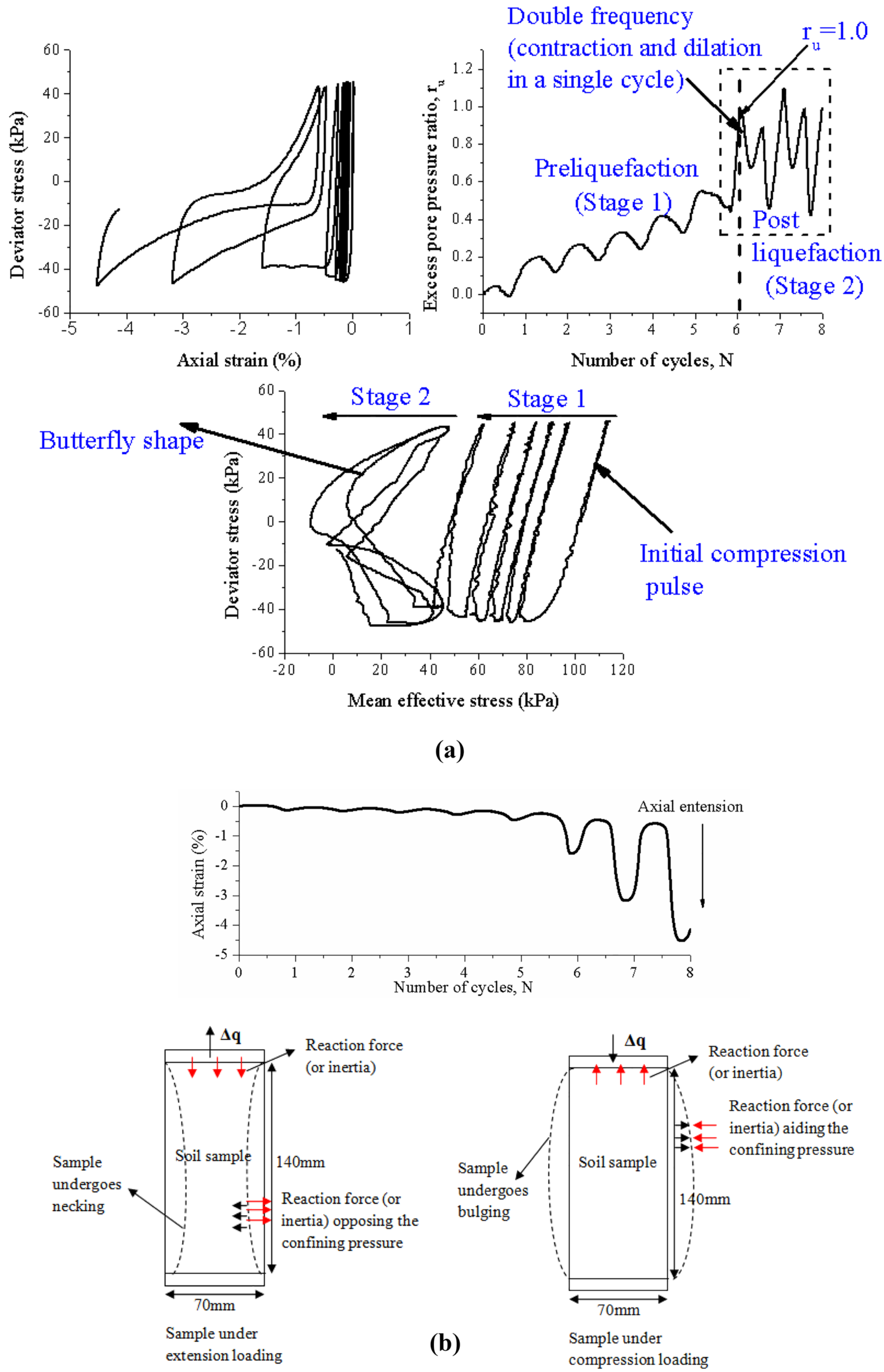
Deviator stress (kPa)
Axial strain (%)
Excess pore pressure ratio, r_u
Number of cycles, N
Double frequency (contraction and dilation in a single cycle)
r_u=1.0
Preliquefaction (Stage 1)
Post liquefaction (Stage 2)
Stage 2
Stage 1
Butterfly shape
Initial compression pulse
Mean effective stress (kPa)
(a)
Axial strain (%)
Axial entension
Number of cycles, N
Δq
Reaction force (or inertia)
Soil sample
140mm
Sample undergoes necking
Reaction force (or inertia) opposing the confining pressure
70mm
Sample under extension loading
(b)
Reaction force (or inertia) aiding the confining pressure
Sample undergoes bulging
Sample under compression loading

◂**Fig. 3** **a** Experimental data (stress–strain loops, pore pressure time history, and effective stress path) on the sand and **b** strain time history and deformation pattern of the sample (modified from Omidvar et al. 2012) during cyclic loading for 60% RD with CSR value of 0.23

sand conducted at 100 kPa confining pressure for RD of 25%, 40, and 60%, and the results are plotted in the same figure. It is observed that the friction angle (drained or undrained) increases with the increase in the relative density of sand for the same confining pressure, which is in line with the past findings (Anderson and Schjetne 2013) in which the variation of friction angle of sand is studied for different relative densities and confining pressures.

The variation of shear wave velocity (or shear modulus) of Kasai river sand with depth (or with the increase in the confining pressure) and changes with relative density is shown in Eq. (1) (Chattaraj and Sengupta 2016).

$$G_{\max} = \frac{611.58(Pa)^{0.532}(\sigma)^{0.468}}{(0.3 + 0.7e^2)} \tag{1}$$

where "e" is the void ratio (which is a function of relative density), "Pa" is the atmospheric pressure (100 kPa), and "σ" is the mean effective stress in kPa. All the cyclic tests are conducted at different relative densities (25%, 40%, 60%, and 80%) of sand with the cyclic stress ratio (CSR) values ranging from 0.10 to 0.33 at an effective confining pressure of 100 kPa with a constant frequency of 1 Hz. The cyclic stress ratio (CSR) is expressed as $q/2\sigma_3$, where q is the deviator stress on the sample and equal to σ_1–σ_3, where σ_1 and σ_3 are the axial and the initial confining stresses, respectively in the triaxial tests. The specimen is consolidated isotropically (equal axial and radial stress) until a Skempton B-value of 0.95 or above is attained (Skempton 1954). This marks the end of the preparation, and the specimen is ready for shearing under deviator loading. The deviator stress (q) is generated by applying an axial strain (ε_a) to the soil. Unless otherwise stated, the deviator stress acting on the sample, q, is equal to (σ_1–σ_3) and the mean effective stress, p, is equal to (σ_1'+2 σ_3')/3 (where $\sigma_2' = \sigma_3'$ are the effective stress). An experimental stress–strain loop and excess pore pressure time history for the sand at 60% relative density (RD) is shown in Fig. 3a.

It may be observed from the experimental stress–strain response that the behavior of the sand is mostly governed by cyclic mobility. The cyclic mobility can occur in both loose and dense sands for a wide range of confining pressure, and it can occur for the states of the soil below or above the critical state line (CSL) in the form of "limited flow" or "no flow" behavior (Kramer 2005). It may be seen that the stress path during cyclic loading gradually shifts toward the origin and the soil contracts predominantly (Stage 1) until the value of r_u reaches unity and it starts to generate typical "butterfly" shape thereby undergoing alternate half cycles of contraction and dilation in a single loading cycle (Stage 2) (post liquefaction) (Zhang and Wang 2012). The cyclic mobility is also associated with the development of strain rate with excursions through transient states of effective confining stress, $\sigma_c' = 0$ in the loading cycles. The existence of double frequency (contraction and dilation in a single cycle) is observed in the pore pressure (u)-time history after the soil reaches initial liquefaction (r_u ~ 1.0). It is observed that for all the samples (with RD 25%, 40%, 60%, and 80%), the axial strain in extension is larger than in compression which results in asymmetric stress–strain loops as shown in Fig. 3a, which are also noted in the past studies conducted on Toyoura sand (Lombardi et al. 2014) and Hostun 31 sand (Zhu et al. 2021). The stress path is inclined toward the right; hence, it initially touches the phase transformation line on the extension side as shown in Fig. 3a. The deformation pattern of the sand sample under compression and extension loading is shown in Fig. 3b which provides an explanation to the asymmetric hysteresis loops in the cyclic triaxial test. In axial extension of the sample, the soil grains tend to move (or slide) away from one another, thereby undergoing necking, and the excess pore pressure ratio decreases in this phase, which is opposite to the compression phase in which the sample bulges and the soil grains move toward each other resulting in the increase in the pore pressure ratio. In the radial direction, the reaction forces oppose the confining stress in the extension phase of the sample which results in a decrease in the overall confining stress on the sample which weakens the resistance to deform (as the frictional force required to slide one grain past another depends upon the effective stress between the two sand grains in contact) and the grains can slide past one another easily which is not observed in the compression phase of the sample in which the confining pressure increases and the sample remains more stable as the resistance to deform increases. Hence, the sample strains more in extension phase than compression phase which is clear from Fig. 3b, which as a result forms asymmetric hysteresis loops.

Figure 4 shows an effective stress path of a monotonic (isotropically consolidated undrained triaxial test) and cyclic triaxial test (with CSR value of 0.23) conducted at RD 60%. The characteristic state or phase transformation (PT) state defines a point in which the behavior of the sand changes from contractive to dilative and is identified by a deviator stress (q) where the excess pore pressure reaches a maximum value on the compression zone. In Fig. 5, the rates of axial deformation in Stage 2 are compared for the sand at RD = 25% (loose sand) and RD = 40% (medium dense sand) with the cyclic stress ratio (CSR) value of 0.18. Initially, both the samples show minimal axial deformations until touching the phase transformation (PT) line, beyond which the loose sand starts to deform excessively. The axial

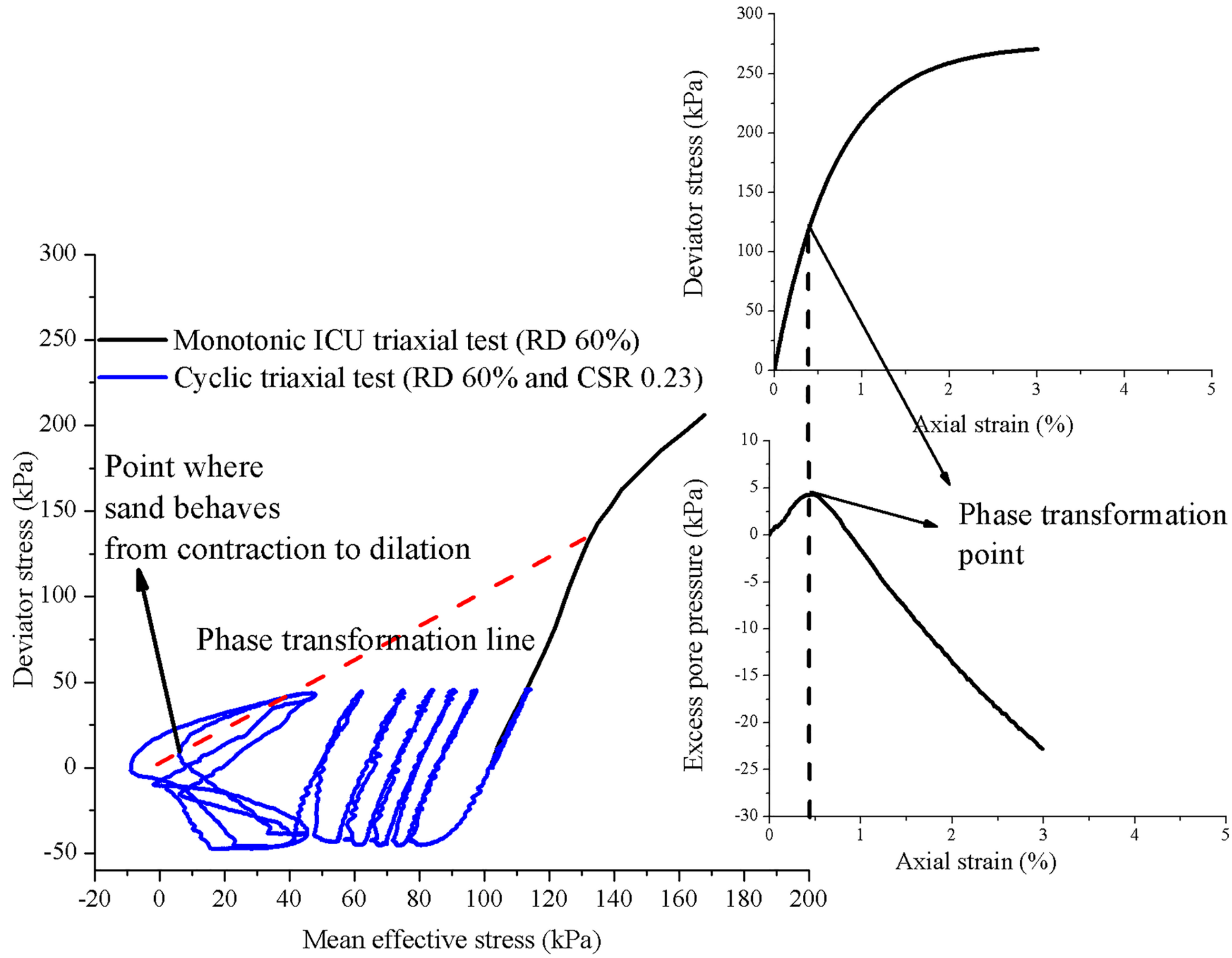

Fig. 4 Monotonic and cyclic triaxial test data (CSR value of 0.23) on the river sand at RD of 60%

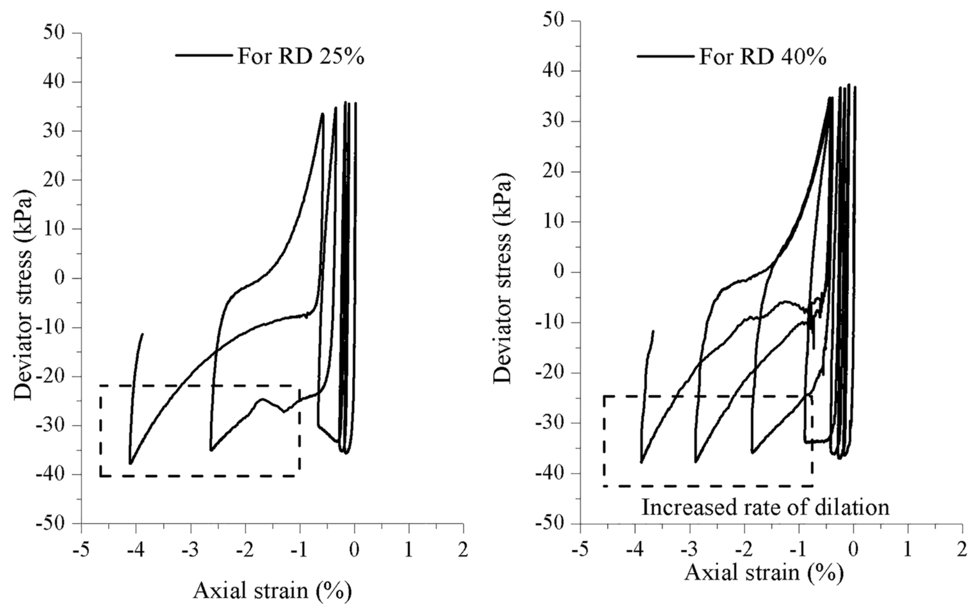

Fig. 5 Experimental stress–strain loops at 25% and 40% RD with CSR value of 0.18

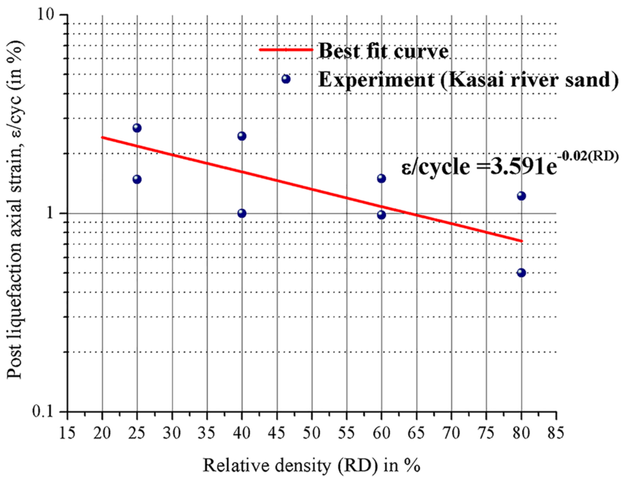

Fig. 6 Variation of post liquefaction axial strain (ε/cycle) variation with relative density for the local sand

deformations develop at a slow rate for the medium dense sand which is also observed in the post liquefaction axial strain accumulation rate. It is observed that the rate of post liquefaction strain accumulation is inversely proportional to the relative density of the sand as shown in Fig. 6. Similar observations have been also reported in the past by Sriskandakumar (2004) for Fraser River sand in the cyclic direct simple shear (DSS) tests. The liquefaction (or cyclic) resistance curve is usually interpreted in CSR-N plane (where CSR is the cyclic stress ratio and N is the applied number of constant amplitude stress cycles). This curve is constructed for the present sand at different relative densities by assuming that liquefaction is triggered when the excess pore pressure ratio (r_u) becomes greater than 0.95. The experimentally obtained points are fitted with a curve fit of the form CSR = aN^{-b} (Boulanger and Idriss 2014) where "a" and "b" are curve fit coefficients which depend on the relative density of the sand. The curve fit parameters of the soil obtained from test results are listed in Table 2.

The present curves are also compared with the cyclic triaxial test data reported on Toyoura sand (Lombardi et al. 2014; Hyodo et al. 1998) and Fraser River sand (Thomas 1992) shown in Fig. 7. It is observed that for a given relative density, the number of cycles to liquefaction (N) increases with decreasing CSR value. Also, for a given number of cycles (N), the CSR value increases with the increase in the relative density (RD) of the sand. This trend is commonly followed in the present study and studies reported in the literature. The relevance of these experimentally obtained curves for liquefaction resistance (CSR v/s N) is that these curves can be used as an input in a simplified liquefaction model proposed by Dawson and Mejia (2012) and Chiaradonna et al. (2018) for simulating the behavior of any type of geo-structures resting on layered soil with different relative densities.

Table 2 Parameters "a" and "b" for river sand

Curve fit parameters	Relative density (%)			
	25%	40%	60%	80%
a	0.235	0.250	0.360	0.410
b	0.132	0.140	0.19	0.195

Numerical models for liquefaction analysis

In this section, a brief description of the two advanced soil constitutive models (Finn-Byrne model and PM4 sand model) for liquefiable soils is discussed.

Finn-Byrne model

The Finn-Byrne liquefaction model (Finn et al. 1977; Itasca 2005) is a loosely coupled effective stress elastic–plastic model which is capable of simulating liquefaction behavior of sands and silts under seismic excitation. The present model is based on Mohr–Coulomb plasticity which is capable of incorporating the effect of Lode angle, which implies that the failure envelope of the soil in tension and compression is different, but the void ratio is kept constant. The primary input parameter of this model is the undrained peak effective friction angle (ϕ_{up}) which is a function of effective confining pressure and relative density of sand. Using this model, it is possible to calculate pore water pressure generation by calculating irrecoverable volumetric strains during dynamic analysis. Byrne (1991) has presented an expression which corresponds irrecoverable volume change ($\Delta\varepsilon_{vd}$) to the engineering shear strain (γ) with two constants:

$$\frac{\Delta\varepsilon_{vd}}{\gamma} = C_1 e^{-C_2 \frac{\varepsilon_{vd}}{\gamma}} \tag{2}$$

where C_1 and C_2 are constants. Byrne (1991) notes that the constant, C_1 and C_2, can be derived from $(N_1)_{60}$, as follows:

$$C_1 = 8.7(N_{1,60})e^{-1.25}$$

and

$$C_2 = 0.4/C_1 \tag{3}$$

where $N_{1,60}$ is the normalized standard penetration test value which is set to correspond to standard penetration test (SPT) measurements and can be related to the relative density of the sand. Also, in this model, a third constant C_3 is introduced to determine the threshold shear strain below which no generation of pore pressure is permitted. The value of C_3 is taken to be zero in the present study. Hence, ϕ_{up}, C_1, C_2,

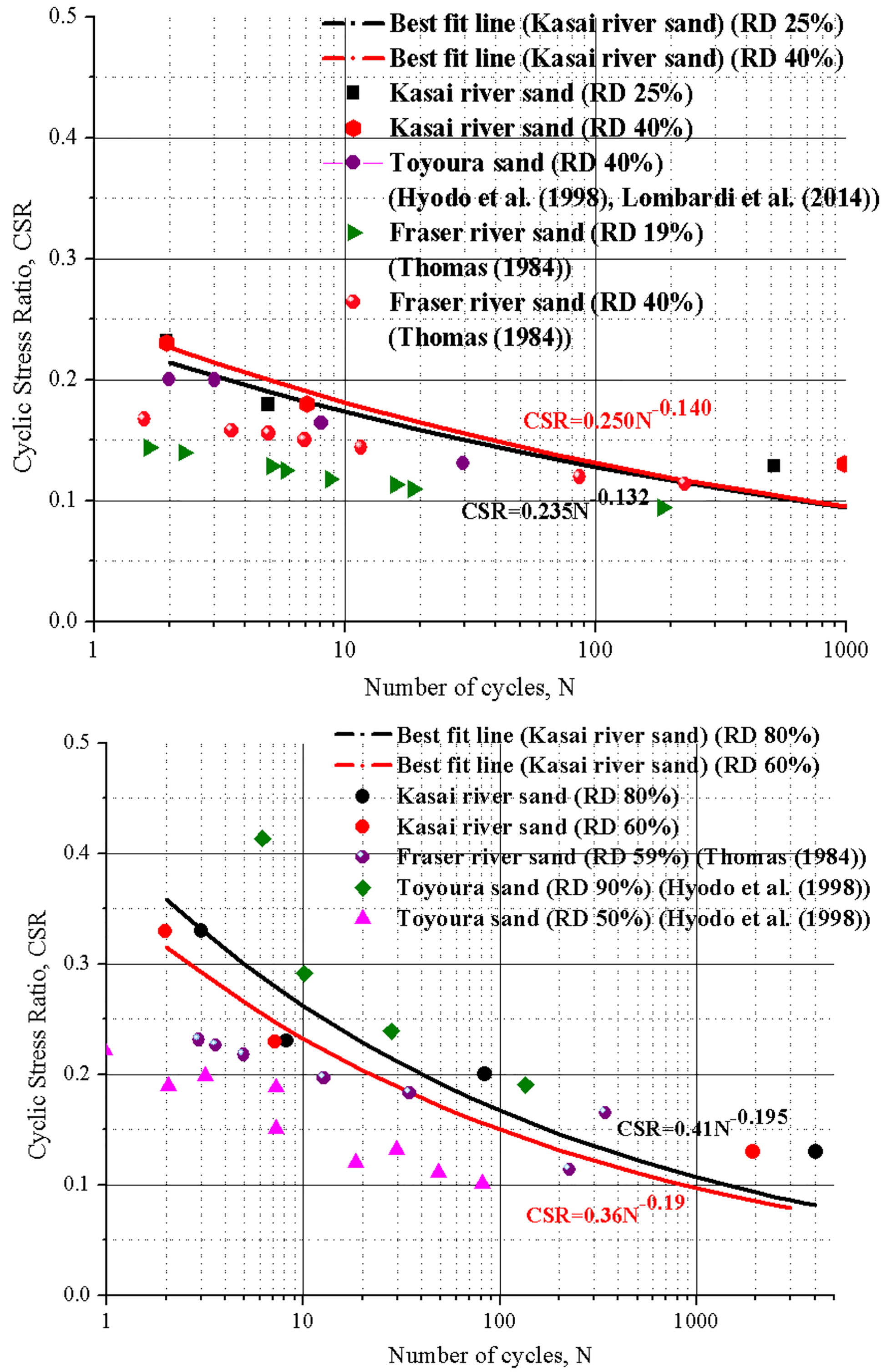

Fig. 7 Liquefaction resistance of the sand at various relative densities

and C_3 are the input parameters required in the Finn-Byrne liquefaction model.

PM4 sand model

The plasticity model for sands or PM4 sand is a stress ratio–controlled critical state bounding surface plasticity model for sand initially proposed by Manzari and Dafalias (1997) and later extended by Dafalias and Manzari (2004).

The present implementation of the model in MIDAS GTS NX (2019) is based on in-plane strains (in 2D). The third, out-of-plane, direction is considered with an elastic evolution in this model formulation. The model takes into account the elastic and the plastic strain increments, which are composed of volumetric and deviator terms.

The elastic strain increments are generated according to the acting stress levels and are restricted by the variable shear modulus, G and the bulk modulus, K of the sand:

$$de^{el} = \frac{ds}{2G}$$

$$de_v^{el} = \frac{dp}{K} \tag{4}$$

The variations of the shear and the bulk moduli (G and K) are given by Eqs. (5) and (6), using a dimensionless constant (G_0); the Poisson's ratio (ν); effective stress, p; and the atmospheric pressure, p_A (utilized for normalization) as

$$G = G_o p_A \left(\frac{p}{p_A}\right)^{1/2} \tag{5}$$

The elastic bulk modulus is related to the shear modulus through the Poisson's ratio as

$$K = \frac{2(1+\vartheta)}{3(1-2\vartheta)} G \tag{6}$$

The value for G_o is estimated for Kasai river sand using Eq. (1). The model is based in terms of the relative state parameter index, $\xi_{cr} = D_{,Rcs} - D_R$, where $D_{,Rcs}$ is the relative density at the critical state, and D_R is the relative density of the soil. The critical surface of the soil is defined by means of the empirical relationship proposed by Bolton (1986) defined by

$$D_{,Rcs} = \frac{R}{Q - \ln(100\frac{p}{p_A})} \tag{7}$$

where the values of the secondary parameters Q and R are the critical state parameters, and p is the mean effective normal stress. In this paper, the state parameter of the present river sand is evaluated by means of the isotropically consolidated undrained/drained triaxial test (ICU and ICD) conduced at RD 25%, 40%, 60%, and 80%. The presently obtained CSL is compared with the different critical state line (CSL) for sands published in the literature as shown in Fig. 8. The value of Q, which is proposed by Bolton (1986) (depends on the type of grains), was maintained at its original value of 10.0, representing soils mainly of quartztic grain properties (Bolton 1986) like Kasai river sand. R is a curve

Fig. 8 Critical state line (CSL) of Kasai river sand along with the initial states of sands in the literature

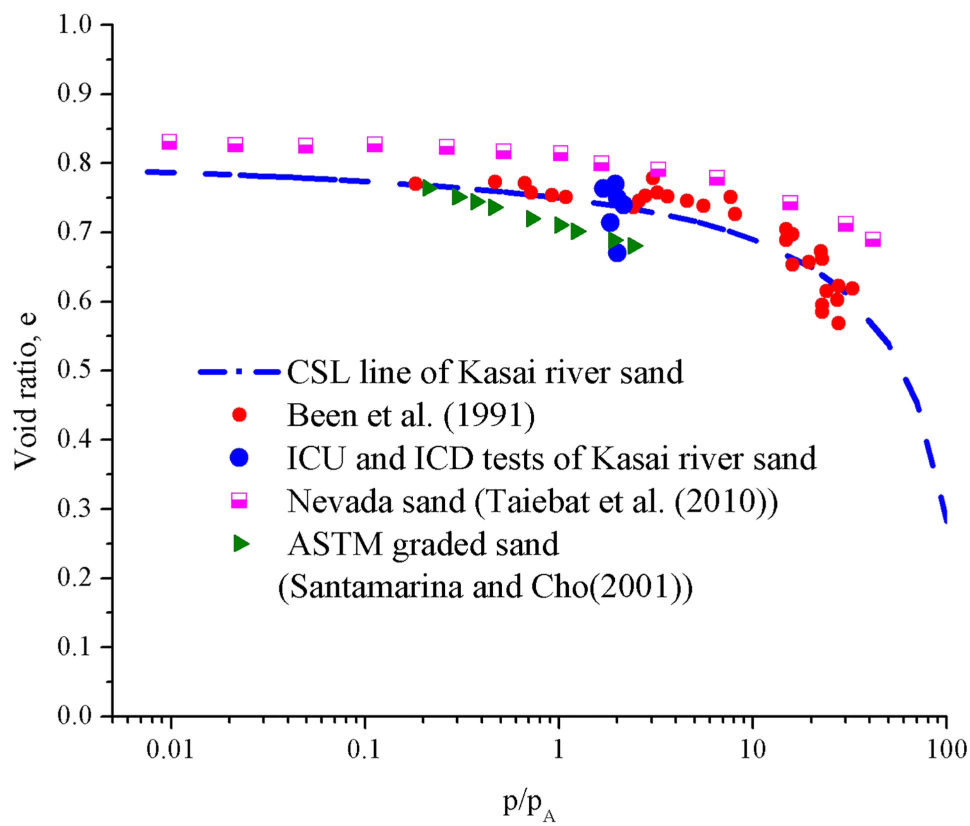

fitting parameter taken as1.5 and is obtained from the CSL line for the river sand in e-log(p/p_A) space (Boulanger 2003) for an effective confining pressure of around 100–200 kPa. Since experimental data at low (< 80 kPa) and high confining pressures (> 200 kPa) is limited for the present sand, the applicability of the present CSL may be inaccurate for those initial states of sand.

For sands which are loose of critical states, the value of $\xi_{cr} > 0$ and $D_{,Rcs} < D_R$ and vice versa. The model utilizes a yield surface defined by Eq. (8), representing a cone in a multiaxial space:

$$f = [(s - p\alpha) : (s - p\alpha)]^{1/2} - \sqrt{\frac{1}{2}}pm = 0 \tag{8}$$

where s is the deviator stress, α is the deviatoric back-stress ratio that characterizes the yield surface axis, and the parameter m controls the size (radius) of the elastic zone of the soil in terms of the stress ratio (= 0.01).

The model uses bounding, dilatancy and critical surfaces according to Dafalias and Manzari (2004). The model does not incorporate Lode angle dependency, and hence, the friction angles are the same for compression and extension loading. The bounding (M_b) and the dilatancy (M_d) ratios are related to the critical stress ratio, M in in-plane stress by the following equations:

$$M = \frac{(\sigma_1 - \sigma_3)}{(\sigma_1' + \sigma_3')/2} = 2 \sin (\varphi_{\mathrm{cv}})$$

$$M_b = M\exp(-n_b\xi_{cr})$$

$$M_d = M\exp(n_d\xi_{cr}) \tag{9}$$

where the model parameters n_b is related to the peak stress ratio in the drained compression test and n_d is related to the phase transformation angle, and these parameters define the computation of M_b and M_d with respect to M. The bounding stress ratio controls the relationship between the peak friction angle and the relative state. During monotonic shearing, the bounding and the dilatancy surfaces approach the critical surface at the same time the relative state parameter index approaches the critical state line.

The bounding surface represents the maximum strength surface (φ_{peak}), and the dilatancy surface defines the location where transformation from contractive to dilative behavior occurs, also known as transformation phase state (PT). The initial location of the bounding surface (M_b), dilatancy surface (M_d) and the critical state surface (M) for the state of a sand in the "loose or dense of critical" is $M_d \geq M > M_b$ and $M_b > M > M_d$, respectively. When the sand is loose of critical, the critical state angle and the dilatancy angle are relatively close to each other. Under undrained cyclic loading, the change in the effective stress is associated with the shear-induced volumetric dilative or contractive tendency of the sand.

This model employs a non-associative flow rule to obtain a realistic evaluation of the plastic strain increments as shown below:

$$d\varepsilon_v^{pl} =< L > D \tag{10}$$

$$de^{pl} =< L > R'$$

where $d\varepsilon_v^{pl}$ is the increment in the plastic volumetric strain, de^{pl} is the increment in the plastic deviator strain. L is the loading index which is defined as $\frac{1}{K_p}\frac{\partial f}{\partial \sigma} : d\sigma$, D is the dilatancy, R is the direction of de_{pl}, R' is the deviatoric component of R, and K_p is the plastic modulus. $< >$ are MacCauley brackets that set negative values to zero (i.e., $<L> = L$ if $L \geq 0$, and $<L> = 0$ if $L < 0$).The tensor R is for the assumption of no Lode angle dependency in the π-plane. The dilatancy D relates the incremental plastic volumetric strain to the incremental plastic deviatoric strain by the relationship

$$d\varepsilon_v^{pl} = D\left|de^{pl}\right| \tag{11}$$

The value of dilatancy (D) is a function of the mean effective stress, deviator stress, initial state of the soil, and relative density (D_R) of soil (Boulanger 2003; Budhu 2011). For a particular value of D_R of the sand, the dilation angle decreases with the increase in the confining pressure (Budhu 2011), which can be observed from the pore pressures near the surface and the bottom of the sand. This can be attributed to the crushing of the grains of the sand. When a sand particle tries to roll over another particle, the grain crushes, and the crushed particles enter into the existing void spaces, thus reducing the dilation tendency. This phenomenon is incorporated in the model by the framework of the well-known stress-dilatancy relationship (Bolton 1986):

$\varphi_{\mathrm{peak}} - \varphi_{cv} = -0.8\psi$ or,

$$\varphi_{\mathrm{peak}} - \varphi_{cv} = -0.8\sqrt{\frac{1}{2}}D \tag{12}$$

where ψ is the angle of dilation. The state dependency of the dilatancy (D) is modeled as $D < 0$ (for $\xi > \xi_{cr}$), $D > 0$ (for $\xi < \xi_{cr}$), and $D = 0$ (for $\xi = \xi_{cr}$). Further details about the calculation of the dilatancy parameter (D) involving Eq. (11) and the state dependency are elaborated in Ziotopoulou and Boulanger (2013) and not elaborated in this study.

The basis of calibration of this model relies on the prediction of site-specific liquefaction resistance curve (CSR v/s N) for all the relative densities under consideration as well as better prediction of pre- and post-liquefaction (which may encompass the post liquefaction strain rate accumulation) response for any set of element test. The model parameters are developed using best-estimated values of unit weight (γ), relative densities (RDs), and G_o which is a dimensionless model constant controlling the small strain shear modulus (G_{max}) obtained from element tests. Other model parameters such as the critical-state friction angle (φ_{cv}), maximum and minimum void ratios (e_{max} and e_{min}), and the parameters Q and R, which define the critical state line in the e-p (or D_R-p) space, are generally found from element tests or reported in Chattaraj and Sengupta (2016). Having defined all the above preliminary parameters (D_R, γ, G_o, e_{max}, e_{min}, Q, R, ϕ_{cv}), the next step is to calibrate the value of n_b (a parameter which controls the peak effective friction angle and dilatancy) which is done by fitting the effective stress path of the model to the butterfly loops in stress space obtained during the experiments, as it relates to the modification of the approach of the bounding surface toward the critical surface thus affecting the value of the minimum excess pore pressure ratio which is experienced during cyclic mobility. The value of h_o (a parameter which adjusts the ratio of plastic to elastic modulus) also affects the pre- and post-liquefaction response of the soil, and it also needs calibration to better match the complete effective stress path obtained during the experiments. Moreover, it also affects the number of cycles to liquefaction. After obtaining the value of n_b and h_o, the parameter h_{p0} (a variable that adjusts rate of contraction) is calibrated by an iterative process to match the target liquefaction resistance curve of the sand at any relative density without compromising the prediction of pre- and post-liquefaction responses of an element test. The calibration of h_{po} should be performed at the end because its values depend on the values assigned to the other parameters. The other secondary parameters (listed in Ziotopoulou and Boulanger 2013) can also be modified during the model calibration for the cyclic tests if it is necessary.

Numerical simulation of the cyclic triaxial tests

A 4-noded plane strain (undrained) quadrilateral element is used to simulate the cyclic triaxial tests of the sand. As the tests are stress controlled, in addition to the initial hydrostatic consolidation effective pressure (= 100 kPa in this study), a cyclic deviator stress (σ_d) at 1 Hz frequency (test frequency) is acting on the element till the liquefaction of the sand (Fig. 9). As stated earlier, two well-established material models, namely, PM4 sand based on bounding surface plasticity (Ziotopoulou and Boulanger 2013) and Finn Byrne model coupled with Mohr–Coulomb criterion (Itasca 2005), are utilized in the numerical analyses. As PM4 sand model

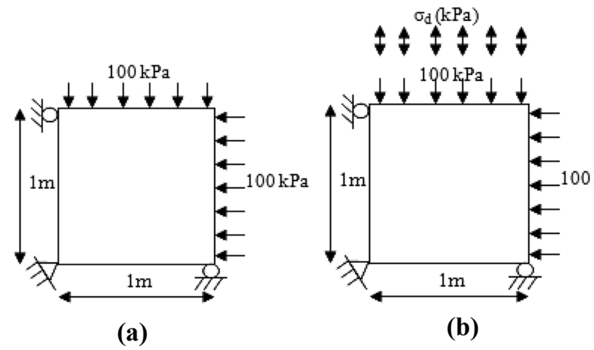

Fig. 9 **a** Initial condition and **b** application of deviator stress during the cyclic tests

is based on in-plane stresses (i.e., out-of-plane stresses are modeled with elastic behavior); hence, the model is limited to plane strain applications only; instead, of modeling the cyclic triaxial test as axisymmetric, it is simulated as plane strain condition (PSC). PSC is a type of simulation in which the two sides are fixed whereas the other two faces are free to move. On the two faces where movement is allowed, the confining pressure (σ_3) remains the same and with the increase in the deviator stress (q), the sample contracts in the direction of the applied deviator stress and tries to expand in the radial direction. Since, in the direction normal to the boundaries in which there is no movement allowed, the sample cannot expand resulting in the increase in the intermediate principal stress ($\sigma_2 = \nu(\sigma_1 + \sigma_3)$, according to the elastic theory) and $\sigma_2 > \sigma_3$. This introduces an additional constraint on the movement of the sand particles which makes rolling more difficult than in triaxial test (where $\sigma_2 = \sigma_3$ in triaxial test). This is a major limitation in this simulation since there is a constraint on an extra degree of freedom of a particle in PS testing. But some studies in the past by Ziotopoulou (2018) and Beaty (2018) have used similar approaches for predicting the cyclic triaxial tests of sand using plane strain compression/extension simulations with sufficient accuracy. As all the numerical simulations are performed in plane strain, the mean effective stress (p) is calculated as $(\sigma_1' + \sigma_3')/2$ for comparison with the experimental observations.

Relationship between fluid bulk modulus and degree of saturation

For dynamic analysis conducted in FLAC 2D (Itasca 2005) or MIDAS GTS NX (2019), if the degree of saturation is less than unity, then the pore pressure is not calculated in those zones. Hence, the indirect way to capture the effect of the degree of saturation on the soil sample is to modify the bulk modulus of water. The relationship between the degree of saturation (S) and Skempton's B-value as proposed by Biot (1962) and Bishop (1973) given as

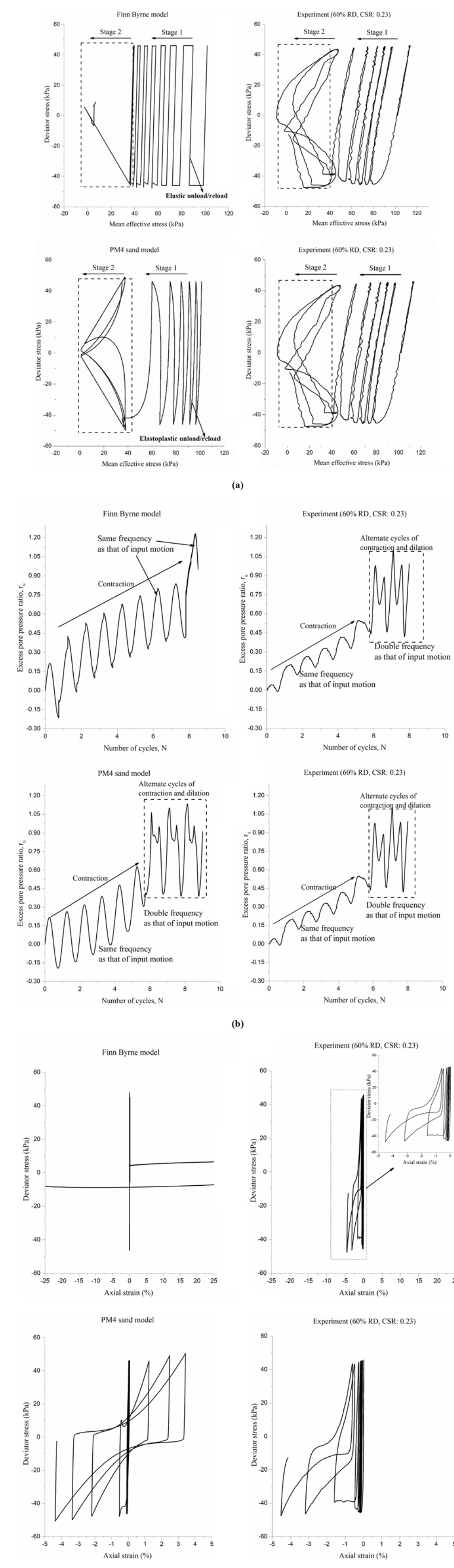

Fig. 10 Comparison between the experimental and the numerical ▸ results using Finn-Byrne model and PM4 sand model for the sand at RD = 60% with CSR value of 0.23

$$B = \frac{\left(\frac{1}{K_b} - \frac{1}{K_s}\right)}{\frac{1}{K_b} - \frac{1+n}{K_s} + \frac{n}{K_w} + \frac{n(1-S)}{u_{abs}}} \tag{13}$$

where K_b is the bulk modulus of the skeleton (calculated in relation to Eq. (1)), K_w is the equivalent bulk modulus of water, K_s is the bulk modulus of the soil grains ($K_s \to \infty$ as the soil grains are assumed to be incompressible), n is the porosity of the soil, u_{abs} is the absolute pore water pressure of the soil ($u_{abs} = u + 100$ kPa, where u is the gauge pressure), S is the degree of saturation. At zero gauge pressure (i.e., pressure above the atmospheric pressure (p_A)), the value of $u_{abs} = 100$ kPa and putting $K_s \to \infty$, the modified relationship is

$$S = 1 - \frac{1 - B\left(1 + n\frac{K_b}{K_w}\right)}{Bn\frac{K_b}{u_{abs}}} \tag{14}$$

In this study, the value of B is kept above 0.95 (Skempton 1954) ensuring saturation of the soil. For the case of RD = 60%, porosity $(n) = 0.40048$, $K_b = 2.14 \times 10^8$ Pa (obtained from Eq. (1)) and $B = 0.9538$ (> 0.95 in the tests), the degree of saturation and the equivalent fluid bulk modulus (K_w) are found to be 99.994% and 1.67×10^9 Pa, respectively. In this equation (Eq. (14)), the values of K_w and S are iteratively chosen to ensure that the B-value of the soil sample becomes more than 0.95.

Using the value of the bulk modulus of water, the pore pressure time history and the effective stress path are obtained from both the models and compared in Fig. 10 with the experimental results for the case of RD = 60%. From Fig. 10, it is observed that the stress path for unloading and reloading predicted by Finn-Byrne model is elastic as the model is based on Mohr–Coulomb failure theory ($q = Mp$, where q is the deviator stress, p is the mean effective confining stress, M is defined as $\frac{6\sin(\varphi_{up})}{3\pm\sin(\varphi_{up})}$, and φ_{up} is the undrained effective angle of internal friction of soil, φ_{up}=39° (obtained from Fig. 2)).The negative sign "−" is for triaxial compression and the positive sign "+" is for triaxial extension. The shear volumetric coupling proposed by Byrne (1991) (parameters $c_1 = 0.16102576$ and $c_2 = 1.2420373$ for $(N_1)_{60} = 14$ (for RD = 60%)) (in Eq. (2)) is added due to which the pore pressure responds to the volumetric change and the effective stress reduces. For the simulation using the Finn-Byrne model, the value of viscous damping ratio of 5% has been assumed, but for PM4 sand model, a value of 1% has been assumed for all the

PSC simulations. The viscous damping ratio simulates the energy dissipation between the soil solids and viscous fluid (water). As PM4 sand model has a small "purely" elastic region (an open-ended yield cone (Eq. (8)) as compared to a relatively large elastic region in the Finn model coupled with Mohr–Coulomb yield criteria, a large value (5%) has been chosen for the Finn model as compared to PM4 sand model (1%) which will have a significant amount of energy dissipation due to hysteresis in relatively smaller strain regime. The dilation angle is always zero, as the volumetric strain predicted by the Mohr–Coulomb model is not considered. This assumption is a convenient one since unrealistically high negative pore pressures may occur due to the use of a positive value of the dilatancy angle, whereas unreasonably large positive pore pressures may develop if the value of the dilatancy angle is negative. With the soil parameters given by $c = 0$ kPa and $\varphi_{up} = 39°$, the applied deviator stress (or shear stress) is less than the shear resistance at the beginning (62.94 kPa, for $\sigma_3' =$ 100 Pa) (see Fig. 10) and hence the soil behaves elastically. After the first 7 cycles of loadings, the effective stress and the shear resistance decrease and at the 8th cycle, the value of the effective stress (σ_3') drops to 38 kPa and the shear resistance becomes 23.90 kPa, which is slightly more than the applied shear stress of 23 kPa ($q/2$). With more loading cycles, the effective stress drops down drastically to zero and the soil liquefies. Once the soil loses its strength, the soil model cannot recover the shear strength with further shearing, and it cannot follow the butterfly shape as observed in the cyclic tests. This can be further confirmed in Fig. 10a. The double-frequency oscillation of pore water pressure as seen in the experiment is not present in the response obtained from the Finn-Byrne model as seen in Fig. 10b, which is a signature of cyclic mobility of a soil. As a result of the dramatic loss in shear strength, there is a sudden increase in shear strain, and the soil fails as seen in the stress strain curve of the Finn-Byrne model in Fig. 10c. Thus, it can be safely concluded that this model is useful for simulating flow liquefaction–induced failures but it is not accurate in predicting the phenomena of cyclic mobility.

In order to overcome the above limitations, a stress ratio and critical state–based bounding surface plasticity model known as PM4 sand is utilized for better simulation of the cyclic mobility as observed in the laboratory cyclic tests. As the unload/reload loops are predominantly elastoplastic, this behavior is simulated by shrinking the size of the yield surface (that is, by making the elastic region to a minimum). A simplified form of the yield surface (an open ended cone) is represented by the expression:

$$f = |\eta - \alpha| - m = 0 \tag{15}$$

In this equation, α is a parameter for kinematic (or rotational) hardening and "m" is a parameter of isotropic hardening. The value of α is related to the variation of plastic

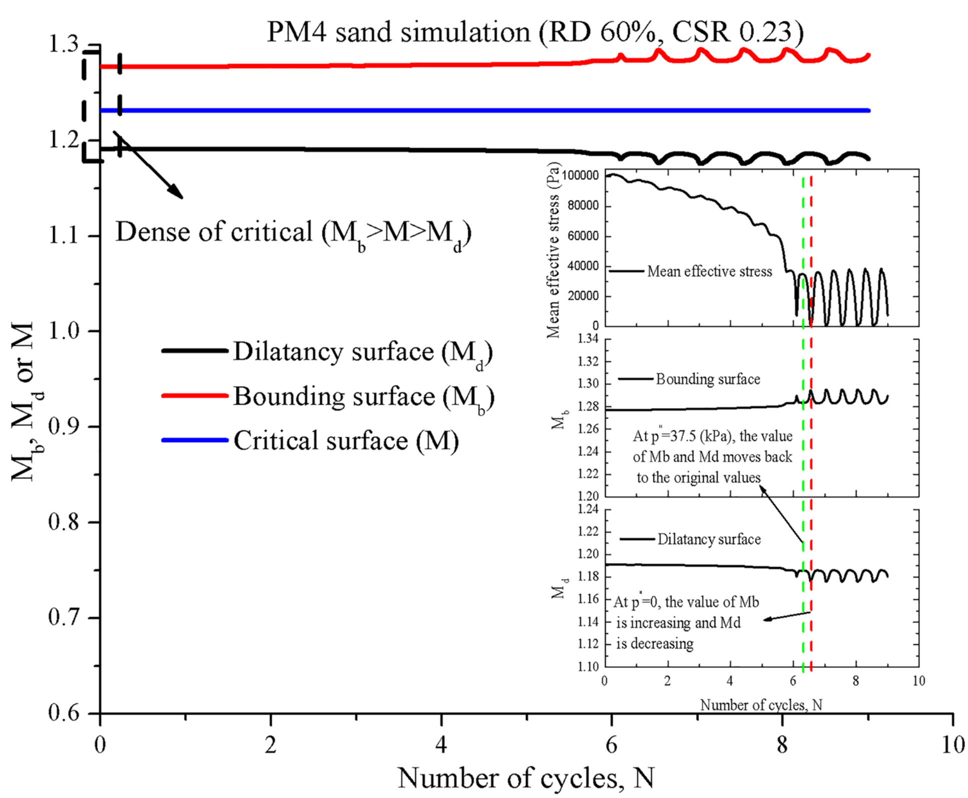

Fig. 11 Evolution of the bounding, critical and dilatancy surface in PM4 sand model with number of loading cycles for CSR value of 0.23 with RD 60%

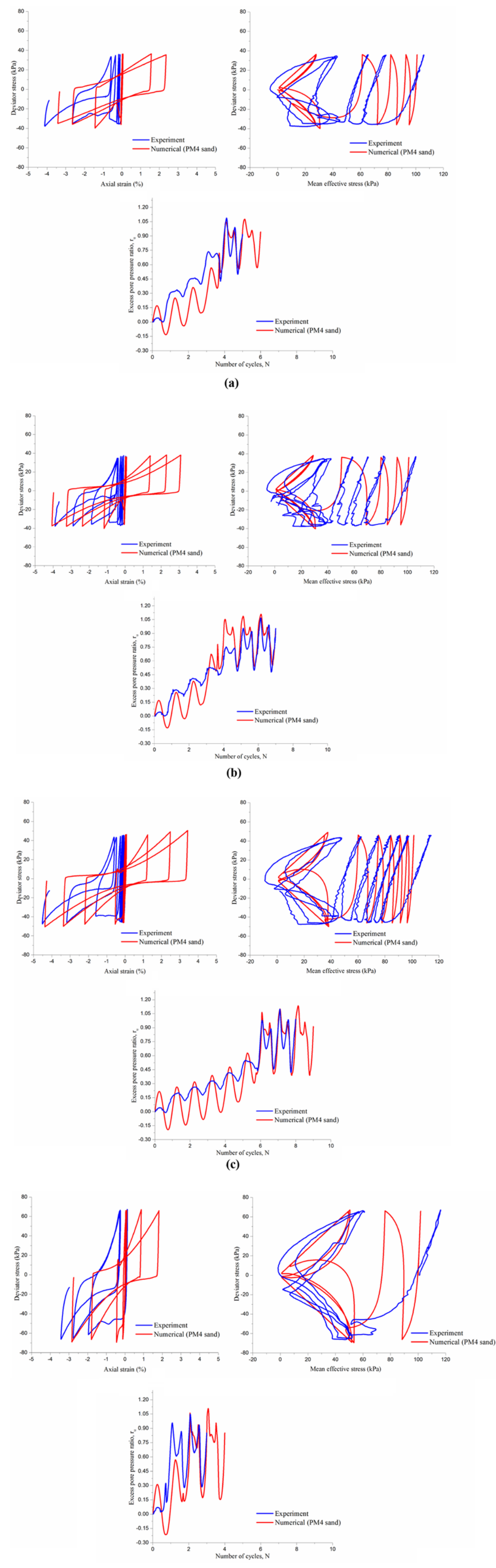

Fig. 12 Comparison of the prediction of PM4 sand model with test data for the sand with **a** RD 25% with CSR value of 0.18, **b** RD 40% with CSR value of 0.18, **c** RD 60% with CSR value of 0.23, and **d** RD 80% with CSR value of 0.33

modulus calculated as per the equation, $K_p = h(M^b - \eta)$, where η is the current stress ratio (q/p), M^b is the image stress ratio on the bounding surface in p-q space, h is a parameter defined in Ziotopoulou and Boulanger (2013). In the above equation, the value of plastic modulus K_p is expressed in terms of the distance of the current stress ratio, η with the image stress ratio, M_b on the bounding surface. In this model, the shear volume coupling is defined in the essence of Rowe's dilatancy theory. and dilatancy $D \left(= d\varepsilon_v^p / |de^p|\right)$is defined (in multiaxial formulation, de^p is the incremental plastic deviator strain and $d\varepsilon_v^p$ is the incremental plastic volumetric strain) in terms of the distance of the current stress ratio η $(=q/p)$ with the image stress ratio M_d on the dilatancy surface. For accurately simulating the phenomena of the cyclic mobility, the dilatancy surface (M_d) acts as a phase transformation point where the behavior of the soil changes from contraction to dilation. For sands with the initial state "loose of critical" $M_b = M < M_d$ and with the initial state "dense of critical" $M_b > M > M_d$, the M_b and M_d gradually converge toward CSL line ($M = 2\sin(\phi_{cv})$, where ϕ_{cv} is the constant volume friction angle of soil) when sheared till the critical state. In PM4 sand model, the definition of dilatancy (D) proposed by Dafalias and Manzari (2004) is modified to incorporate the effects of fabric and fabric history and to improve the relationship between CRR and the number of uniform loading cycles and to avoid the stabilization problem in effective stress path when it becomes close to the failure surface at $p = 0$, as pointed out by Dafalias and Manzari (2004) in their original model (Ziotopoulou and Boulanger 2013).

With these modifications, the results predicted in terms of effective stress path, time history of pore pressure ratio, and the stress strain response is compared in Fig. 10a–c. All the relevant features including predicting the post liquefaction response are predicted accurately in this model. Figure 11 shows the evolution of the three surfaces (namely critical state (a function of ϕ_{cv}), bounding, and dilatancy surface (a function of relative state parameter, ξ_{cr})) with the number of loading cycles. It is observed from Figs. 11, 10b that after 6 cycles of loading, when r_u is close to 1.0, the relative state parameter decreases which results in an increase of the stress ratio of the bounding surface (M_{b}) and decrease of dilatancy surface (M_d). In addition, after 6 cycles of loading, when r_u is close to 0.375, the state parameter increases back to the

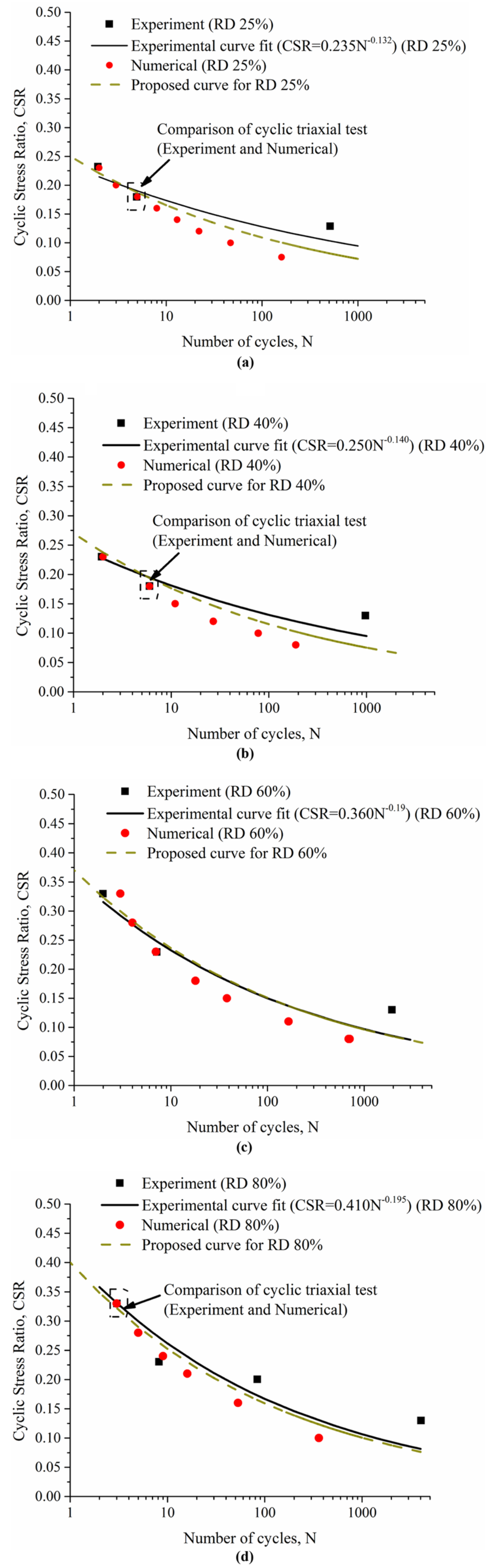

Fig. 13 Comparison of the liquefaction resistance curves obtained ▶ from PM4 sand model with test data for **a** 25%, **b** 40%, **c** 60%, and **d** 80% relative density (RD)

original value due to which the stress ratio of M_b and M_d move back to their original values.

From Fig. 11, it may be seen that the constant difference between the bounding and the dilatancy surface might result in shear locking or ratcheting which hinders development of large strains (Dafalias and Manzari 2004; Tasiopoulou and Gerolymos 2016). The PM4 sand overcomes these problems by (a) the modification of the fabric effects (fabric dilatancy tensor as a function of plastic deviator strain) which was initially introduced by Dafalias and Manzari (2004) as a function of the plastic volumetric (dilational) strain and (b) incorporating the fabric terms in the shear modulus (G) (ref Eq. (5)), plastic modulus (K_p) and dilatancy term (D) (in both contraction and dilation phase) simultaneously (Ziotopoulou and Boulanger 2013). The variables $C\varepsilon$ and z_{cum} (bounded by the value of $z_{\max}$) included in the fabric dilatancy tensor in the PM4 sand (Ziotopoulou and Boulanger 2013) adjust the rate of accumulation of post liquefaction strains and ensure that the undrained stress strain loops progressively accumulate with strains. These parameters are calculated internally corresponding to each state of stress in the model. Thus, the introduction of the fabric effects in the PM4 sand further improves the performances in predicting post liquefaction axial (or shear) strains as observed in Fig. 10c (or Fig. 12) in which the axial strain of PM4 sand model is not underestimated as compared to the experimental data. The numerical simulation using PM4 sand model shows symmetric loops, and experimental results show asymmetric loops. This difference between the numerical and experimental results arises due to the different loading paths between the plane strain condition in numerical simulation and the triaxial loading condition existing in experiments. Hence, PM4 sand is found to be more efficient in predicting the cyclic behavior

Table 3 Calibrated parameters of PM4 sand for the given sand

Parameters	Values			
D_R (apparent relative density)	25%	40%	60%	80%
$e_{\min}$ (Table 1)	0.56	0.56	0.56	0.56
$e_{\max}$ (Table 1)	0.83	0.83	0.83	0.83
G_o (Eq. (1))	864.00	922.40	995.80	1015.50
Q (Fig. 8)	10	10	10	10
R (Fig. 8)	1.5	1.5	1.5	1.5
n_b (controls the bounding ratio)	0.78	0.22	0.11	0.11
ϕ_{cv} (constant volume friction angle)	38	38	38	38
h_{po} (controls the rate of contraction)	1.575	0.4	0.2	0.015
h_o	0.32	0.32	0.32	0.45

Table 4 Parameters for river sand and values reported by Rad and Clough (1982)

Curve fit parameters	Relative density (%)					
	25% (present sand)	25% rad and clough (1982)	40% (present sand)	40% rad and clough (1982)	60% (present sand)	60% rad and clough (1982)
a	0.235	0.17	0.270	0.28	0.370	0.550
b	0.18	0.14	0.185	0.145	0.195	0.290

of sand (mainly the phenomena of post liquefaction), and the remaining cyclic tests are simulated using this model. The parameters of PM4 sand (namely n_b, h_{po}, and h_o) modified by trial and error to predict the pre- and post-liquefaction behavior of cyclic tests on the sand are tabulated in Table 3. The values of the other model parameters (reported in Ziotopoulou and Boulanger 2013) are kept as default.

The stress–strain curve, pore water pressure time history, and effective stress path obtained from PM4 sand model are compared with the test data at only one CSR value for each relative density in Fig. 12a–d. From Fig. 12a–d, it is observed that the phenomena of cyclic mobility and the rate of post liquefaction axial strain accumulation are accurately reproduced. The double-frequency oscillation of pore water pressure is also reproduced with great accuracy by PM4 sand model. It is to be noted that as the simulations are conducted as plane strain compression and extension, the asymmetric nature of the hysteresis loops is not properly captured as observed in the cyclic triaxial tests. Figure 13 shows the numerical comparison of the experimentally obtained liquefaction resistance curves. From the figures, it is observed that the curvature of the liquefaction resistance plot (CSR v/s N) is predicted accurately for all the relative densities of sand, but a prevalent problem is the underestimation of liquefaction resistance at higher number of cycles for all the relative densities of sand. The misfit of liquefaction resistance at large cycles creates a problem during the dynamic simulation of a free field soil column or a SSI phenomenon including liquefaction subjected to low amplitude of seismic excitation. As the low amplitude of seismic excitation will create low shear stress (or low CSR) in the soil column, the model will predict quick liquefaction (or the rate of generation of pore pressure will be more) as compared to the actual observation (Dawson and Mejia 2012). This will subsequently create an overestimation of the settlement prediction of sand (or structure resting over sand), and the design will be conservative. To alleviate the problem, an ideal case would be to match the liquefaction resistance curve (CSR v/s N) of the soil for all the stress amplitude cycles such that the prediction of pore pressure and subsequent rate of strength degradation of soil is predicted correctly for all the stress amplitudes, thus highlighting the importance of liquefaction resistance curve which is a signature of the soil under undrained cyclic loading.

In addition, the equations of CSR v/s N are proposed for all four relative densities which encompass the points obtained from experimental and numerical simulations as shown in Fig. 13. The equations proposed are listed in Eqs. (16)–(19) which are meant for fully saturated sand ($B > 0.95$):

$$CSR = 0.25(N)^{-0.180} \text{ For 25\% RD} \tag{16}$$

$$CSR = 0.27(N)^{-0.185} \text{ For 40\% RD} \tag{17}$$

$$CSR = 0.37(N)^{-0.195} \text{ For 60\% RD} \tag{18}$$

$$CSR = 0.40(N)^{-0.200} \text{ For 80\% RD} \tag{19}$$

The obtained values of a and b are compared with the literature values obtained for cohesionless soil as reported in Rad and Clough (1982) as shown in Table 4. From the table, it is seen that the values of the curve fit parameters a and b depend on the type of sand (i.e., the grain size distribution and its initial fabric); hence, these values depend on the type of sand under consideration. The authors propose these equations for the present sand which can be used as an input in a simplified liquefaction model proposed by Dawson and Mejia (2012) and Chiaradonna et al. (2018) for simulating the behavior of any type of geo-structures resting on top of this sand while incorporating proper correction factors for initial static shear stress or overburden pressures.

Conclusions

The present study calibrates two liquefaction models namely Finn-Byrne model and PM4 sand using the cyclic triaxial experiments on Kasai river sand. It is found that the Finn model predicts well up to the point of initial liquefaction, but it is not as good in predicting the phenomena of cyclic mobility (post liquefaction) which is accompanied by alternate contraction or dilation of the sand specimen.

This problem is dealt with great accuracy in PM4 sand model by introducing the concept of phase transformation line (or dilatancy line) and fabric dilatancy tensor which help in improving the predictive capability of pre- and post-liquefaction phenomena of a sand to a great extent.

As the Finn-Byrne model is based on the Mohr–Coulomb failure theory, the failure surfaces on compression and extension are different which signifies lode angle dependency which is absent in PM4 sand model.

The proposed liquefaction resistance curves of CSR v/s *N* (number of stress amplitude cycles) for different relative densities of Kasai river sand are obtained from PM4 sand model and validated using experimental data. The proposed curves can be used for obtaining the liquefaction potential of any type of sand having properties (i.e., C_u, C_c, D_{50}, etc.) similar to Kasai river sand. The proposed curves give accurate prediction of the liquefaction resistance with *N* for all the relative densities of sand. But for a large number of cycles, it gives lesser resistance than actually observed and is thus conservative. Furthermore, instead of going for a detailed numerical simulation using PM4 sand model, the proposed curves for liquefaction resistance (CSR v/s *N*) can be utilized in a simplified liquefaction model proposed by Dawson and Mejia (2012) and Chiaradonna et al. (2018) for simulating the behavior of any type of geo-structures.

Acknowledgements The authors' work was benefitted from the electronic discussions held with Associate Prof. Nikos Gerolymos at National Technical University of Athens. The authors of the paper would also like to thank the reviewers for their time and for the thought provoking comments which helped to improve the quality of the work.

Author contribution All the authors contributed to the study. The experiments were performed by Rana Chattaraj (as a part of his Ph.D. work) and Raj Banerjee (as a part of his M. Tech work) under the guidance and supervision of Prof. Aniruddha Sengupta which was validated numerically in the present study. The first draft of the manuscript was written by Raj Banerjee and Dr. Yogita Parulekar, and the authors commented on previous versions of the manuscript. All the authors read and approved the final manuscript.

Funding Fellowship received from Bhabha Atomic Research Centre, Mumbai, for the first author during Masters (M. Tech) at IIT Kharagpur.

Availability of data and material All the experimental data and the numerical simulations that support the findings of this study are available from the corresponding author upon reasonable request.

Code availability The numerical simulations as a part of this study were performed in FLAC 2D and MIDAS GTS NX.

Declarations

Competing interests The authors declare no known competing interests.

References

Anderson KH, Schjetne K (2013) Database of friction angles of sand and consolidation characteristics of sand, sit, and clay. Journal of Geotechnical and Geoenvironmental Engineering ASCE 139(7):1140–1155

Arulanandan K, Scott RF (1993) Verification of numerical procedures for the analysis of soil liquefaction problems. Vol. 1: experimental results and numerical predictions. Int. Conf. on the Verification of Numerical Procedures for the Analysis of Soil Liquefaction Problems. Rotterdam, Netherlands: A.A. Balkema.

Arulanandan K, Scott RF (1994) Verification of numerical procedures for the analysis of soil liquefaction problems. Vol. 2: experimental results and numerical predictions. Int. Conf. on the Verification of Numerical Procedures for the Analysis of Soil Liquefaction Problems. Rotterdam, Netherlands: A.A. Balkema.

ASTM D5311 (2011) Test method for load controlled cyclic triaxial strength of soil. Annual book of ASTM standards, ASTM International West Conhohocken PA.

Aubry D, Hujeux JC, Lassoudiere F, Meimon Y (1982) A double memory model with multiple mechanisms for cyclic soil behavior. Int. Symp. on Num. Models in Geomechanics, Zurich, (ed) R. Dungar, G. N. Pande and J. A. Studcr. Balkerna, Rotterdam.

Beaty M, Byrne PM (1998) An effective stress model for predicting liquefaction behavior of sand. Proceedings of a specialty conference, Geotechnical Earthquake Engineering and Soil Dynamics ASCE 766–777

Beaty MH (2018) Application of UBCSAND to the LEAP centrifuge experiments. Soil Dyn Earthq Eng 104:143–153

Biot MA (1962) Mechanics of deformation and acoustic propagation in porous media. J Appl Phys 33:1482–1498

Bishop AW (1973) The influence of an undrained change in stress on the pore pressure in porous media of low compressibility. Géotechnique 23(3):435–442

Bolton MD (1986) The strength and dilatancy of sands. Géotechnique 36:65–78

Boulanger RW (2003) High overburden stress effects in liquefaction analyses. Journal of Geotechnical and Geoenvironmental Engineering ASCE 129(12):1071–1082

Boulanger RW, Idriss IM (2014) CPT and SPT based liquefaction triggering procedures. Davis, CA: Center for Geotechnical Modeling, Department of Civil andEnvironmental Engineering, University of California; Report No. UCD/CGM-14/01

Budhu M (2011) Soil mechanics and foundation, 3rd edn. John Wiley & Sons Inc, Hoboken

Byrne PM (1991) A cyclic shear-volume coupling and pore pressure model for sand. Proceeding of Second International Conference on Recent Advances in Geotechnical Earthquake Engineering and Soil Dynamics 1:47–55

Carey TJ, Kutter BL (2017) Comparison of liquefaction constitutive models for a hypothetical sand. Geotechnical Front (GSP 281)

Chattaraj R, Sengupta A (2016) Liquefaction potential and strain dependent dynamic properties of Kasai River sand.Soil Dyn. Earthq Eng 90:467–475

Chen L, Ghofrani A, Arduino P (2020) Prediction of LEAP-UCD-2017 centrifuge test results using two advanced plasticity sand models. In: Kutter B., Manzari M., Zeghal M. (ed) Model Tests and Numerical Simulations of Liquefaction and Lateral Spreading. Springer.

Chiaradonna A, Tropeano G, d'Onofrio A, Silvestrim F (2018) Development of a simplified model for pore water pressure build-up induced by cyclic loading. Bull Earthq Eng 16(9):3627–3652

Dafalias YF, Manzari MT (2004) Simple plasticity sand model accounting for fabric change effects. J Engg Mech ASCE 130(6): 622–634

Dawson EM, Mejia LH (2012) Updates to a practice-oriented liquefaction model. GeoCongress; ASCE 2118–2127

ElgamalA YZ, Parra E (2002) Computational modeling of cyclic mobility and post-liquefaction site response. Soil Dyn Earthq Eng 22(4):259–271
Eslami MM, Zarrabi M, Yniesta S(2019) Evaluation of two constitutive models in predicting the cyclic behavior of a natural clay. 7th Int Conf Earthq Geotechnical Eng 2275–2282
Finn WLD, Lee KW, Martin GR (1977) An effective stress model for liquefaction. J Geotech Eng Div ASCE. https://doi.org/10.1061/AJGEB6.0000434
Ghaboussi J, Dikmen SU (1978) Liquefaction analysis of horizontally layered sands. J Geotech Eng Div ASCE 104(GT3): 341–356
Hyodo M, Hyde AFL, Aramaki N (1998) Liquefaction of crushable soils.Geotechnique 48(4): 527–543
Itasca Consulting Group, FLAC (2005) Fast Lagrangian analysis of continua in 2-dimensions 5.0, manual. Itasca, Minneapolis.
Jefferies M, Been K (2015) Soil liquefaction: a critical state approach. CRC Press
Kramer SL (2005) Geotechnical earthquake engineering.Prentice hall, Upper Saddle River, NJ.
Kutter BL, Carey TJ et al (2015) LEAP database for verification, validation, and calibration of codes for simulation of liquefaction. In Proc., 6th Int Conf Earthq Geotechnical Eng. Christchurch, New Zealand.
Lombardi D, Bhattacharya S, Hyodo M, Kaneko T (2014) Undrained behavior of two silica sands and practical implications for modelling SSI in liquefiable soils. Soil Dyn Earthq Eng 66:293–304
Manzari MT, Dafalias YF (1997) A critical state two-surface plasticity model for sands. Géotechnique 47(2): 255–272
MIDAS G (2019) GTS NX User Manual.
Mroz M (1967) On the description of anisotropic work-hardening. J Mech Phys Solids 15:163–175
Omidvar M, Iskander M, Bless S (2012) Stress-strain behavior of sand at high strain rates. Int J Impact Eng 49:192–213
Parra E (1996) Numerical modeling of liquefaction and lateral ground deformation including cyclic mobility and dilation response in soil system. Dissertation, Rensselaer Polytechnic Institute.
Prevost JH (1985) A simple plasticity theory for frictional cohesionless soils. Soil Dyn Earthq Eng 4(1):9–17
Rad NS, Clough WG (1982) The influence of cementation on the static and dynamicbehavior of sands. The John A. Blume Earthquake Engineering Center, Stanford Univ., Report No, Stanford, California, p 59
Ramirez J, Barrero AR, Chen L, Dashti S, Ghofrani A, Taiebat M, Arduino P (2018) Site response in a layered liquefiable deposit: evaluation of different numerical tools and methodologies with centrifuge experimental results. J Geotechnical Geoenvironmental Eng ASCE 144(10): 04018073
Shou KJ, Wang CF (2003) Analysis of the Chiufengershan landslide triggered by the 1999 Chi-Chi earthquake in Taiwan. Eng Geol 68(3):237–250
Skempton A (1954) The pore-pressure coefficients A and B. Geotechnique 4:143–147
Sriskandakumar S (2004) Cyclic loading response of Fraser Riversand for validation of numerical models simulating centrifuge tests. Dissertation, University of British Columbia.
Stark TD, Contreras IA (1998) Fourth Avenue landslide during 1964 Alaskan earthquake. Journal of Geotechnical and Geoenvironmental Engineering ASCE 124(2):99–109
Tasiopoulou P, Gerolymos N (2016) Constitutive modeling of sand: formulation of a new plasticity approach. Soil Dyn Earthq Eng 82:205–221
Thomas J (1992) Static, cyclic and post liquefaction undrained behavior of Fraser River sand. Dissertation, University of British Columbia.
Wu W, Bauer E, Kolymbas D (1996) Hypoplastic constitutive model with critical state for granular materials. Mech Mater 23(1): 45–69
Xenaki VC, Athanasopoulos GA (2003) Liquefaction resistance of sand-mixtures: an experimental investigation of the effect of fines. Soil Dyn. Earthq Eng 23:183–194
Yang M, Seidalinov G, Taiebat M (2018) Multidirectional cyclic shearing of clays and sands: Evaluation of two bounding surface plasticity models. Soil Dyn Earthq Eng 124:230–258
Yang Z, Elgamal A, Parra E (2003) Computational model for cyclic mobility and associated shear deformation. J Geotechnical Geoenvironmental Eng ASCE 129(12): 1119–1127
Zarrabi M, Yniesta S (2019) Recent Advanced Constitutive Models for Liquefaction and Cyclic Softening Analysis.72nd Canadian Geotechnical Conference, At: St. John's, Newfoundland and Labrador, Canada.
Zhang JM, Wang G (2012) Large post-liquefaction deformation of sand, part I: physical mechanism, constitutive description and numerical algorithm. Acta Geotech 7(2):69–113
Zhu Z, Zhang F, Peng Q, Dupla JC, Canou J, Cumunel G, Foerster E (2021) Effect of the loading frequency on the sand liquefaction behaviour in cyclic triaxial tests. Soil Dyn Earthq Eng 147: 106779
Zienkiewicz OC, Chang CT, Hinton E (1978) Non-linear seismic response and liquefaction. Int J Numer Anal Meth Geomech 2:381–404
Ziotopoulou K (2018) Seismic response of liquefiable sloping ground: class A and C numerical predictions of centrifuge model responses. Soil Dyn Earthq Eng 113:744–757
Ziotopoulou K, Boulanger RW (2013) Calibration and implementation of a sand plasticity plane-strain model for earthquake engineering application. Soil Dyn Earthq Eng 53:268–280